Separation and Purification Technology 270 (2021) 118793

Contents lists available at ScienceDirect

Separation and Purification Technology

journal homepage: www.elsevier.com/locate/seppur

Theoretical and practical approach to the dealcoholization of water-ethanol mixtures and red wine by osmotic distillation

Javier Esteras-Saz [a,b], Óscar de la Iglesia [a,b,c], Cristina Peña [d], Ana Escudero [d], Carlos Téllez [a,b], Joaquín Coronas [a,b,*]

[a] Instituto de Nanociencia y Materiales de Aragón (INMA), CSIC-Universidad de Zaragoza, Zaragoza 50018, Spain
[b] Chemical and Environmental Engineering Department, Universidad de Zaragoza, Zaragoza 50018, Spain
[c] Centro Universitario de la Defensa Zaragoza, Academia General Militar, 50090 Zaragoza, Spain
[d] Laboratorio de Análisis del Aroma y Enología (LAAE), Department of Analytical Chemistry, Universidad de Zaragoza, Instituto Agroalimentario de Aragón (IA2) (UNIZAR-CITA), Associate Unit to Instituto de las Ciencias de la Vid y el Vino (ICVV) (UR-CSIC-GR), Zaragoza 50009, Spain

ARTICLE INFO

Keywords:
Wine dealcoholization
Osmotic distillation
Polypropylene membrane
Hollow fiber
Modeling
Hansen solubility parameters

ABSTRACT

Osmotic distillation (OD) has been a subject of interest during the last few years due to its promising application in the production of low alcohol strength wines. This work focuses on the partial dealcoholization (-3 v/v%) of red wine (tempranillo) by OD, carrying out an experimental and theoretical process analysis. The dealcoholization process was performed using a polypropylene hollow fiber module at different experimental conditions whose influence in the ethanol behavior was evaluated. At the best tested conditions, the study of the behavior of ethanol and other five different alcohols (both aliphatic and aromatic) as a function of their volatility (Henry's constant) and their interaction with the membrane (in terms of Hansen solubility parameters) validated the theoretical model proposed. As a result, a transport resistance expression that includes the alcohol-membrane interaction was successfully developed. This allowed to reduce the error between the experimental and theoretical alcohols concentrations in a relatively wide range of working conditions.

1. Introduction

There is growing evidence that a climate change is taking place, whose impact extends well beyond an increase of Earth temperature. It is also affecting the stability of ecosystems and communities around the world [1–3]. Viticulture has been also affected, since in recent years changes in the annual cycle of vine have been observed, which leads to a temporal mismatch between industrial and phenolic maturity [4].

The degree of ripeness conferring the optimal flavor characteristic of wine normally correlates with the highest sugar content in grapes. However, due to the global warming, the juice obtained from grapes at full phenolic maturation has an excessive concentration of sugar, resulting in wines with undesirably higher concentrations of ethanol [5]. This phenomenon is aggravated in warm climate areas such as the Mediterranean region, particularly including France, Italy and Spain as main producers of wines, and it is expected to be intensified in the next years [6,7]. Also, it has been suggested that the temperature increase (which could go from 0.3 to 1.7 °C during the next 20 years), consequence of global warming, may affect gene expression and enzymatic activity which determine grape ripening and wine characteristics [8].

At this moment, in the Mediterranean region, most of the red wines already exceed 14 v/v%, and an increment of 2 v/v% of ethanol has been detected in wines from California [9]. Furthermore, in the past twenty years, the alcoholic strength of Australian wines increased from 12.4 v/v% to 14.4 v/v% for red wines and from 12.5 v/v% to 13 v/v% for white ones [10]. As an additional example, based on the daily average air temperature data from 1981 to 2017, it was concluded that Ningxia region in China will have to change the wine grape varieties and wine types to adapt to the ongoing climate change [11].

During must fermentation, ethanol is produced with other substances such as esters, glycerol or succinic acid that confer the wine their organoleptic interest [12]. An excessive ethanol concentration is undesirable since it increases the solubility of the volatile compounds in the wine, masking the main aromas and increasing the perception of hotness on the mouth, thus reducing the wine quality [13,14]. Besides, the growing social tendency towards a healthy lifestyle, avoiding an excess of alcohol consumption, has resulted in an increasing demand of wines with lower ethanol content, and there is no doubt that less alcoholic wines (e.g. 2–3° below the current ones) would have a positive reception

* Corresponding author at: Instituto de Nanociencia y Materiales de Aragón (INMA), CSIC-Universidad de Zaragoza, Zaragoza 50018, Spain.
E-mail address: coronas@unizar.es (J. Coronas).

https://doi.org/10.1016/j.seppur.2021.118793
Received 21 January 2021; Received in revised form 13 April 2021; Accepted 13 April 2021
Available online 18 April 2021

Nomenclature

A	Membrane area of the hollow fibers (m^2)
C	Concentration (g kg^{-1})
d	Diameter (m)
D	Effective diffusion (m^2s^{-1})
G	Mass of a component (g)
Gz	Graetz number: $Gz = ReScd_h/L$
H	Henry Constant (Pa m^3 mol^{-1})
HSP	Hansen solubility parameter ($MPa^{0.5}$)
J	Partial flux (g s^{-1} m^{-2})
K	Mass transfer coefficient
K_f	Feed mass transfer coefficient (m s^{-1})
K_G	Global mass transfer coefficient (g m^{-2} s^{-1} Pa^{-1})
K_s	Stripping mass transfer coefficient (m s^{-1})
K_m	Membrane mass transfer coefficient (g m^{-2} s^{-1} Pa^{-1})
L	Effective length of the module (m)
M	Molar weight (g mol^{-1})
n	Number of hollow fibers
Q	Flow rate (mL min^{-1})
R_f	Feed mass transfer resistance (s Pa g^{-1})
R_m	Membrane mass transfer resistance (s Pa g^{-1})
R_s	Stripping mass transfer resistance (s Pa g^{-1})
Re	Shell side Reynolds number: $Re = 4Q_i/\mu_i n\pi d_i$ (dimensionless)
R_g	Ideal gas constant (8.314 J mol K^{-1})
Sc	Schmidt number: $Sc = D_i/v$ (dimensionless)
Sh	Sherwood number (dimensionless)
T	Temperature (K)
t	Time (s)
v	Molar volume (cm^3 mol^{-1})
V	Volume (mL)
W	Weight (g)

Greek letters

δ	Membrane thickness (m)
δ_d	Dispersion force of Hansen solubility parameters ($MPa^{0.5}$)
δ_h	Specific interaction of Hansen solubility parameters ($MPa^{0.5}$)
δ_p	Polar interaction of Hansen solubility parameters ($MPa^{0.5}$)
ε	Membrane porosity (dimensionless)
μ	Fluid viscosity (Pa s)
ν	Kinematic viscosity: $\nu = \mu/\rho$ (m^2 s^{-1})
ρ	Fluid density (kg m^{-3})
τ	Membrane tortuosity (dimensionless)
υ	Fluid velocity (m s^{-1})
φ	Variable in Eq. (13)
ϕ	Packing density (dimensionless)

Subscripts

a	Inner of the module
co	Outer of the central collector tube
e	Effective
ex	External
Exp	Experimental
f	Feed phase
G	Global
h	Hydraulic
in	Inner
k	Knudsen
ln	Logarithm mean
m-air	Molecular in air
p	Pore membrane
s	Stripping phase
Theo	Theoretical

Superscripts

EtOH	Ethanol
i	Component
w	Water

from markets and consumers. For this reason, decreasing the ethanol content of the current wines maintaining suitable organoleptic profiles, adequate preservation properties and healthier is currently one of the most important issues for the wine community [4,15,16].

To adapt to the above described situation of global warming in the context of wine production but also to satisfy the consumer demand and produce fresh and balanced wines with low alcoholic strength, different strategies have been studied [17,18]. Currently the most popular dealcoholization techniques are focused on the removal of ethanol from finished wines with post-fermentation separation treatments such as spinning cone columns and reverse osmosis [19,20]. However, during the separation carried out with spinning cones the wine must be slightly heated, causing an energy cost and a possible modification of its organoleptic properties. Moreover, reverse osmosis requires a relatively high energy consumption to raise the required pressure, while the installation cost can be important due the high membrane area needed to achieve a desired production. As an alternative, osmotic distillation (OD) can produce an ethanol reduction working at room temperature and with no pressure gradient thanks to the use of hydrophobic membranes. As a consequence of the low working temperature, OD has a tolerable energy demand and a low impact on the composition and sensory attributes of the processed wines. Several works have been published on the OD application for low-alcohol wine production where a partial dealcoholization did not influence significantly the color, total anthocyanins, flavonoids and contents of phenols [21,22].

In OD process, a hydrophobic porous membrane, typically of polypropylene, acts as a contactor, with the liquid mixture containing ethanol in the feed side and the extracting agent (stripper, usually liquid water) in the permeate side. The hydrophobic character of the membrane prevents water transport, while the other components of the feed that diffuse through the membrane pass from liquid to vapor phase inside the matrix pores. As a result, the gradient of partial pressures of these components between both membrane sides contributes to the driving force for the separation, meaning a reduced loss of minor components comparing to other techniques mentioned above.

The reduced loss of minority compounds during OD has been evidenced for most acids and phenolic compounds (anthocyanins and tannins) as previously reported [21,22]. However, the loss of some volatile compounds is inevitable. Lisanti et al. reported a loss of around 40% esters with a partial (-2 v/v%) dealcoholization of wine [23]. While a loss up to 80% was observed by Corona et al. during a dealcoholization of 5 v/v% [22]. In fact, in dealcoholization processes where wines with an alcoholic graduation less than 1 v/v% were obtained the relative loss of volatile compounds was as high as 98% [21].

In light of these results, the need to gain more insight into the ethanol behavior and its influence on the volatile components of wine during OD is evident. Recently, several theoretical approaches based on the classical resistance in series model [24,25] were applied [26–28] to describe the evolution of ethanol and aromas in the membrane contactor. However, this model, based only on the volatility to describe the liquid-gas distribution of components, was not able to predict significant differences as a function of the flow rate [27]. This may be due to the fact that

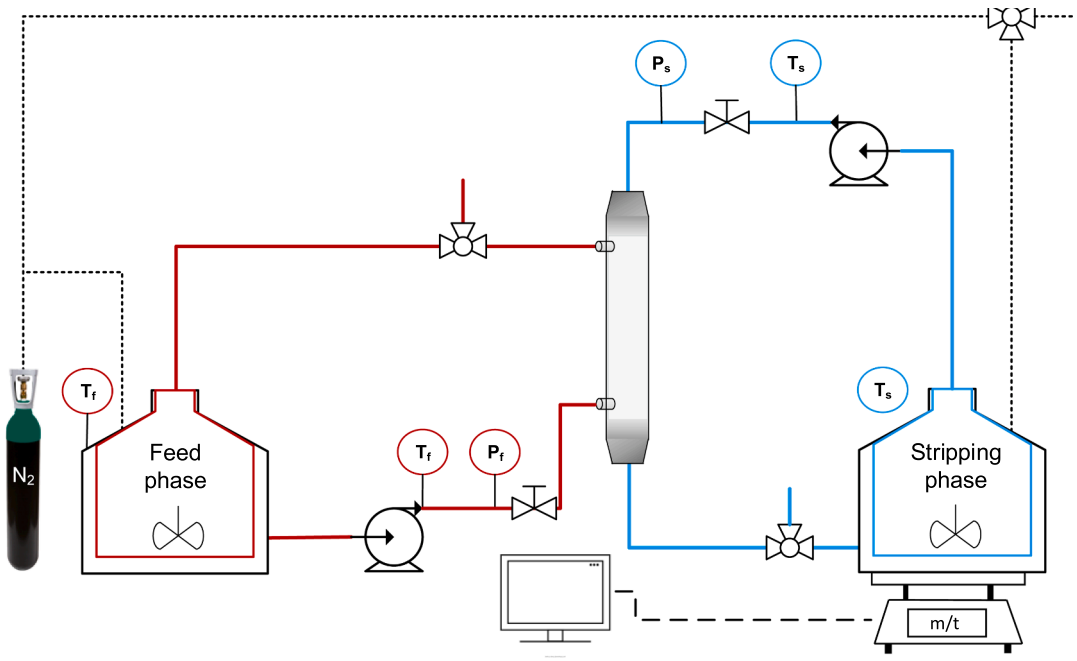

Fig. 1. Osmotic distillation lab scale plant scheme. T_f, T_s thermocouples, P_f, P_s manometers.

Table 1
Characteristics of the hollow fiber membrane module (MM - 1x5.5 x-50 Liqui-Cel™) as supplied by the manufacturer 3M™.

Membrane module parameter	Value
Effective membrane area (m^2)	0.18
Number of fibers	2300
Nominal pore size (μm)	0.03
Porosity (-)	0.4
Tortuosity (-)[a]	2.5
Effective fiber length (cm)	14
Membrane thickness (μm)	40
Internal fiber diameter (μm)	220
External fiber diameter (μm)	300

[a] Estimated by the following equation:$\tau = 1/\varepsilon$.

Table 2
Operating conditions at room temperature (21 °C) and V_f = 375 mL.

Condition	Q_f ($mL \cdot s^{-1}$)	Q_s ($mL \cdot s^{-1}$)	V_s (mL)	V_f/V_s
1	65	39	75	5
2	65	39	375	1
3	65	39	187.5	2
4	21	39	187.5	2
5	40	39	187.5	2
6	74	39	187.5	2

Q_f feed flow rate, Q_s stripping flow rate, V_f feed volume, V_s stripping volume.

the role of the membrane in the separation mechanism was not almost addressed. In this work, our main objective is to shred some additional light into the wine dealcoholization with hydrophobic membranes. With this purpose, first, a correlation between the OD of water-ethanol solutions and red wine will be assessed. Second, a set of experiments using wine as feed stream will be carried out to obtain the operation conditions that yield the best performance in terms on ethanol permeation and short contact time to minimize loss of aromas. Third, a mathematical model integrating the component-membrane interaction based on the application of Hansen solubility parameters will be developed, focusing on the evolution of individual wine components apart from ethanol. Finally, the experimental OD will be compared with the results generated by the proposed model at different working conditions.

2. Materials and methods

2.1. Experimental setup

Fig. 1 shows the schematic representation of the lab scale plant for the osmotic distillation (OD) experiments. This includes the membrane module with the feed (Q_f) and stripping (Q_s) flow systems, pressure and temperature sensors and a scale for continuous monitoring of permeation.

The feed tank, containing 375 mL of red wine (tempranillo, which corresponds to a black grape variety mainly grown in Spain) that was kindly provided by Bodegas Matarromera (Valbuena del Duero, Valladolid, Spain), is connected to the shell side of the membrane module. The stripping tank, with an adjustable volume between 75 and 375 mL of water, is connected to the tube side of the membrane module and both streams circulate in a counter-current configuration. This configuration facilitates the membrane operation. The recirculated feed and stripping streams are continuously fed into the module by peristaltic pumps (DINKO, model 1.9735.15) with flows varying from 21 to 74 mL min^{-1}.

The membrane module was equipped with Liqui-Cel™ MM-1x5.5 hydrophobic porous polypropylene (PP) hollow fiber membranes from 3M™. The main characteristics of the membrane module are detailed in Table 1.

The morphological characteristics of the PP hollow fibers were observed by scanning electron microscopy (SEM) using a microscope Inspect™ F50 model working at a voltage of 10 kV.

The temperatures of feed and stripping phases are measured by K-type thermocouples. All the experiments were carried out at room temperature (21 °C). Two manometers (MEX3D820B15, Bourdon) measure the pressure at tube and shell sides yielding values close to 1 atm. The stripping tank is placed on an electronic precision scale (PRACTUM1102-1S, Sartorius) with a readability of 0.01 g to register its weight every 60 s since the beginning of each experiment. This allows to have an accuracy estimation of the mass flow through the membrane as a function of time, i.e. a continuous monitoring of the dealcoholization process. The different volumes, flow rates and temperature of both

streams used in this study are detailed in Table 2.

During the experiments, 1 mL samples of the two streams leaving the module were taken at constant time intervals to analyze their ethanol concentration. 20 μL of methanol (HPLC grade, Scharlau) was added to each sample as internal standard. 0.5 μL of this mixture was injected on a gas chromatograph 7820A (Agilent Technologies) equipped with a PORAPAK Q80/100 column, 2 m × 1.8 in × 2 mm and FID detector. The injector worked in splitless mode with a ratio 1:100 at 250 °C. Helium was used as carrier gas at a constant flow of 1 mL min^{-1} and the temperature in the oven was fixed at 200 °C. After each experiment, the aroma compounds in the partial dealcoholized wines were analyzed following a procedure previously developed and validated [29].

From the ethanol concentration of samples and stripping weight, mass flows at fixed time intervals were calculated following this equation (Eq. (1)):

$$J_{Exp}(t) = \frac{\Delta W}{A_e \Delta t} \tag{1}$$

Where ΔW is the variation of mass in the stripping or ethanol amount in the feed stream for an interval of time, Δt. Fixed time intervals were used for the previous calculations due to the fact that working in a recycle mode process decreases the driving force across the membrane as a function of time, what in turn reduces the ethanol flux through the membrane.

After each experiment, the membrane module was cleaned as follows. Milli-Q water was fed through the tube and shell sides for 20 min. Subsequently, a 0.5 v/v% NaOH solution preheated at 40 °C was recirculated at 65 mL min^{-1} for 15 min through both membrane sides. Then the system was rinsed again with Milli-Q water using the same flow without recycling for 15 min. Finally, the membrane module was dried in two steps: first vacuum drying was applied at room temperature during 2 h using a PFEIFFER vacuum pump (MVP-040–2). After that, nitrogen was forced to flow through the membrane during 30 min at 100 cm^3(STP) min^{-1} to ensure that the membrane pores were completely dried.

3. Theory

As previously stated, during OD ethanol is transferred from the wine towards the stripping stream (water) through a hydrophobic hollow fiber membrane contactor. Due to the hydrophobicity of the membrane, the aqueous streams at both membrane sides are not in contact through the pores, thus a liquid-vapor interface is formed in each pore edge. This vapor-liquid equilibrium distribution between the feed phase-air and striping phase-air can be considered by means of the respective Henry's constant, H^i. In fact, recent studies suggest that the Henry's constant values correlate with the loss of volatile organic compounds (VOCs) from the wine through the membrane [26,27,30]. Therefore, the flux of each volatile component across the membrane in osmotic distillation, J^i (g m^{-2} s^{-1}), can be expressed as (Eq. (2)):

$$J^i = K_G^i \left(\frac{\rho_f H_f^i}{M^i} C_f^i - \frac{\rho_s H_s^i}{M^i} C_s^i \right) \tag{2}$$

where K_G^i (g m^{-2} s^{-1} Pa^{-1}) is the global mass transport coefficient and C_f^i and C_s^i are the concentrations of components in the feed and stripping sides, respectively.

K_G^i is inversely proportional to the global resistance to the mass transfer; and R_G^i is given by the sum of the three mass transfer resistances involved in the process (Eq. (3)): mass transfer resistance in the feed boundary layer, R_f^i, mass transfer resistance through the air gap in the membrane pores, R_m^i, and mass transfer resistance in stripping boundary layer, R_s^i [24,25].

$$R_G^i = R_f^i + R_m^i + R_s^i \rightarrow \frac{1}{A_e K_G^i} = \frac{H^i}{A_{in} M^i K_f^i} + \frac{1}{A_{lm} K_m^i} + \frac{H^i}{A_{ex} M^i K_s^i} \tag{3}$$

As a minor simplification, same values of Henry constant were considered in the feed and stripping sides when applying the previous equation.

The mass transfer coefficients in the stripping, K_s, and feed, K_f, boundary layers can be calculated for each component from the Sherwood number, with the following expression (Eq. (4)):

$$Sh^i = \frac{K^i d_h}{D^i} \tag{4}$$

where D_i is the molecular diffusion coefficient in the liquid phase (m^2 s^{-1}), and d_h is the hydraulic diameter (m), which can be described by Eq. (5) as a function of the inner diameter of the module, d_a, the outer diameter of the central delivery tube, d_{co}, the external diameter of the hollow fibers, d_{ex}, and the number of hollow fibers, n.

$$d_h = \frac{4 cross - sectional\ area\ of\ flow}{total\ fiber\ external\ circumference} = \frac{d_a^2 - d_{co}^2 - n d_{ex}^2}{d_a + n d_{ex}} \tag{5}$$

Here, the structure of the module did not show a central collector tube. Therefore, d_{co} value is 0 in the equation presented above.

Sherwood number can be predicted by using correlations of the general form of Eq. (6):

$$Sh^i = A f(\phi) \left(\frac{d_h}{L} \right)^{\alpha} Re^{\beta} Sc^{\gamma} \tag{6}$$

where A, α, β and γ are constants from the correlation of experimental data as a function of ϕ, which is the packing density of the module. Re and Sc are Reynolds and Schmidt numbers, respectively (see below).

Regarding the stripping stream boundary layer, Lévêque correlation is widely used in the literature to predict the tube or stripping side mass transfer [31]. However, its limit of validity in terms of Graetz number, Gz, is not well defined. In the present work, Eq. (7) was chosen to predict Sh^i since a value of $Gz = 3.24$ was obtained and this equation is recommended when Gz is less than 6 [32].

$$Sh_s = 0.5 Re Sc \left(\frac{d_h}{L} \right) \tag{7}$$

The mass transfer coefficient in the feed boundary layer on the shell side was calculated using the correlation of Shen et al. [33], Eq. (8), since the constraints of the correlation correspond to the current experimental conditions ($0.1 < Re < 250$; $0.32 < \varnothing < 0.45$).

$$Sh_f = 0.055 Re_f^{0.72} Sc^{0.33} \tag{8}$$

Mass transfer resistance of the membrane can be obtained from the so-called dusty gas model [34]. This model considers that the ethanol diffusion mechanism into the membrane pore is led by the Knudsen diffusion (molecule-pore wall collisions) and molecular effective diffusion (molecule-molecule collisions). Hence, the membrane transport coefficient in the membrane pores is expressed as (Eq. (9)):

$$K_m^i = \frac{M^i \varepsilon}{R_g T \delta \tau} \left[\frac{1}{D_k^i} + \frac{1}{D_{m-air}^i} \right]^{-1} \tag{9}$$

Where ε and τ are the membrane porosity and tortuosity respectively, M^i is the molar weight of component i, T is the absolute temperature in K at which the experiment is carried out, R_g is the ideal gas constant, and D_{m-air}^i is the molecular effective diffusion estimated with the Fuller, Schettler and Giddings relation [35] (Eq. (10)):

$$D_{m-air}^i = \frac{10^{-3} T^{1.75} \left(\frac{1}{M^i} + \frac{1}{M^{air}} \right)^{\frac{1}{2}}}{P \left[\left(\sum v^i \right)^{\frac{1}{3}} + \left(\sum v^{air} \right)^{\frac{1}{3}} \right]^2} \tag{10}$$

where v^i and v^{air} are the diffusion volumes (cm^3 mol^{-1}) for

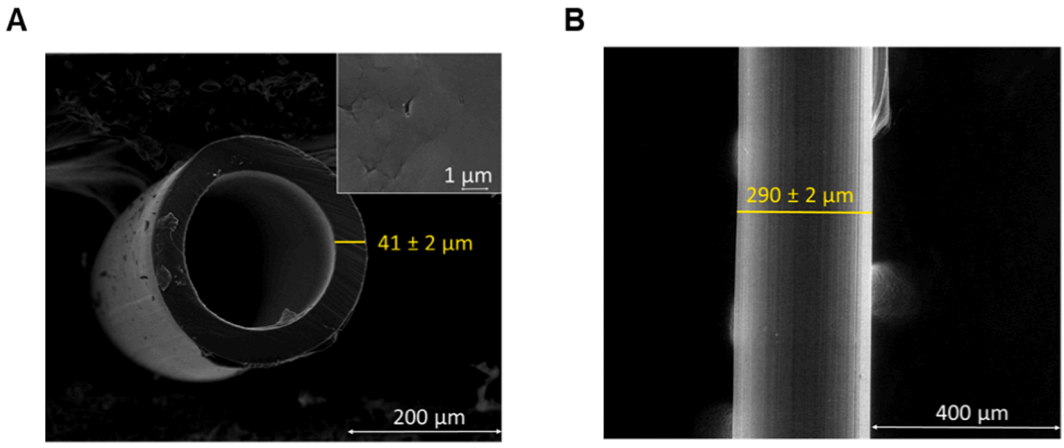

Fig. 2. Hollow fiber membrane cross-section (A) and external surface (B) SEM images of MM - 1x5.5 x-50 Liqui-Cel™ hollow fiber. The inset of (A) shows a detail of the membrane cross section.

components i and air, respectively.

Finally, Knudsen effective diffusion, D_k^i, is typically calculated with the following equation:

$$D_k^i = \frac{d_p}{3}\left(\frac{8R_gT}{\pi M^i}\right)^{1/2} \tag{11}$$

where d_p is the pore diameter of the hollow fibers. It is noticeable that this diffusion was found negligible in the case of aroma compounds [27,36]. Therefore, the molecular effective diffusion leads its behavior through the membrane, and the mass transfer coefficient of the membrane is expressed as follows:

$$K_m^i = \frac{M^i \varepsilon D_{m-air}^i}{R_g T \delta \tau} \tag{12}$$

The influence of the interaction of each wine component with the membrane in terms of solubility, which is expected to contribute in some extent to the prediction of the components behavior during OD, is described here by the application of Hansen solubility parameters, *HSP*. These parameters integrate the dispersion force, δ_d, polar interaction (dipole-dipole), δ_p, and specific interaction such as hydrogen bonding, δ_h [37,38]. To predict the solubility of each component (1) on the membrane (2) the following expression can be used:

$$HSP = \left[(\delta_{d2} - \delta_{d1})^2 + (\delta_{p2} - \delta_{p1})^2 + (\delta_{h2} - \delta_{h1})^2\right]^{1/2} \tag{13}$$

where values of δ_{di}, δ_{pi} and δ_{hi} of each component and membrane polymer were obtained from previous literature [39] (Supplementary Table S1). In fact, we propose the modification of previous equation (3) by introducing the *HSP*, within the global mass transfer resistance expression as follows:

$$R_G^i = R_f^i + R_m^i + R_s^i \rightarrow \frac{1}{A_e K_G^i} = \frac{H^i}{A_{in} M^i K_f^i} + \frac{1}{A_{lm}\left[\frac{HSP^i}{HSP^w}\right]^{\varphi_i} K_m} + \frac{H^i}{A_{ex} M^i K_s^i} \tag{14}$$

Here, each individual *HSP* is standardized with respect to membrane-water *HSP*. It is worth mentioning that the influence of this wine component-membrane interaction would be different for every component or family of components. Therefore, φ parameter, whose value would depend on each chemical family present in the wine (alcohols, esters and acids), is included in the expression. This modified model was applied to several alcohols, including ethanol, whose global mass transfer coefficients were properly defined and calculated accordingly (Supplementary Tables S2 and S3). Its further application to the rest of the volatile components is under study.

The calculations of the model were implemented through an Excel sheet from Microsoft Office Professional Plus 2016 applying the following procedure. Given the experimental system described above, the driving force across the membrane decreases as a function of time. This means that concentrations and fluxes of each component change with time. Knowing K_G^i by means of the theoretical model and the initial component i concentration in feed, the initial J^i (t = 0) is calculated using equation (2). This permeation flux allows us to obtain the mass of component i transferred and the new volumes of the feed and stripping phases, applying the boundary conditions corresponding to the membrane module and the volumes and flow rates used, after an infinitesimal time. Then, new concentrations in both phases can be obtained to recalculate the permeation flux of the component i for the next infinitesimal time. The calculation finishes when the dealcoholization time observed in the experimental section is reached.

4. Results and discussion

4.1. Hollow fiber module characterization

Fig. 2 depicts the SEM images of one of the hollow fibers conforming the membrane module where it is possible to see its internal and external (290 ± 2 µm) diameter together with the membrane thickness (41 ± 2 µm). Besides, Fig. 2A and B show the cross-section and external surface of the hollow fiber, respectively. Membrane thickness and inner and outer diameters are in agreement with those provided by the module marketer. In addition, the inset in Fig. 2A shows the membrane cross-section at a higher magnification, where a relatively homogeneous morphology is observed.

4.2. Osmotic distillation of water – ethanol

To study the performance of the OD set up, several preliminary experiments were carried out feeding water-ethanol solutions for dealcoholization. To accurately estimate the ethanol flow through the membrane from the stripping weight monitoring, each condition was replicated three times (Supplementary Tables S4 and S5). Indeed, the chromatographic analysis of ethanol at intervals of ca. 10 min that supported these studies demonstrated that the gain of weight in the striping reservoir corresponded to ethanol (Supplementary Figures S1 and S2 for the different working conditions in Tables S4 and S5) within experimental error.

In addition, the good correlation of the ethanol behavior during the OD process with hydroalcoholic solutions with that observed with wine in previous reports [26,28] was confirmed here, allowing to use these results in further OD experiments with wine as feed (Supplementary

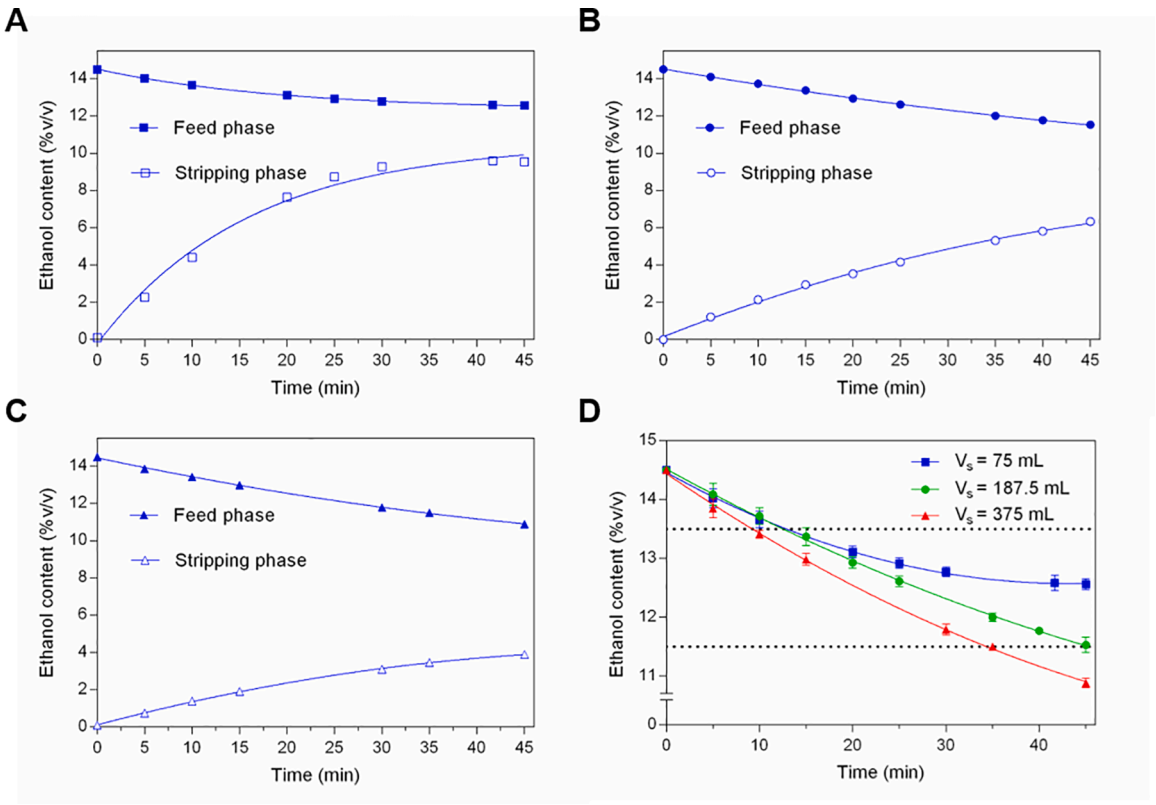

Fig. 3. Ethanol content as a function of time corresponding to a wine feed with 14.5 v/v% of ethanol. (A) $V_f/V_s = 5$; (B) $V_f/V_s = 2$; (C) $V_f/V_s = 1$; (D) Simultaneous comparison of ethanol content in the feed phase at different volume conditions. $V_f = 375$ mL; temperature = 21 °C; $Q_f = 65$ mL min^{-1}; $Q_s = 39$ mL min^{-1}. Represented data are the mean values with the corresponding standard deviations from a triplicated analytical measurement. The curves are only guides to the eye. Solid and open symbols correspond to feed and stripping sides, respectively.

Table S6).

4.3. Influence of feed/stripping volume ratio

Once the OD operation was validated with water-ethanol solutions, red wine was submitted to partial dealcoholization using the same experimental set up. With the goal of a decrease in the alcoholic degree of 3 v/v% (i.e. from the initial 14.5 v/v% to 11.5 v/v%), the volume ratio of both feed/stripping streams (V_f/V_s) was revealed as a critical variable in the operation of the OD carried out in this work. For a constant volume of feed phase, V_f, of 375 mL, volumes of stripping phase, V_s, between 75 and 375 mL were used. Fig. 3A-3C show the variation of the ethanol content in the feed and stripping streams with time for different V_f/V_s ratios. For an accurate comparison, Fig. 3D plots together the three curves of alcohol content in the feed. As the stripping volume increased, a higher loss of alcohol towards the stripping water was obtained under the same operation time. The alcohol content-V_f/V_s-time interaction suggests that it is possible to plan the achievement of a certain degree of alcohol in a relatively short period of time, what would minimize the wine exposure to conditions that may alter its properties. Besides the operation was done at near 20 °C.

It is noticeable that at $V_f/V_s = 5$ (condition (1) in Table 2), the ethanol reduction was similar to those of the other ratios up to 20 min, and after that moment this operation condition limited the dealcoholization. This was due to the fact that the rapid decrease in the concentration gradient between feed and stripping streams, reaching almost steady state ($J_{Exp}^{EtOH} = 0$) and preventing from achieving the degree of dealcoholization proposed (-3 v/v%). Moreover, no important difference in the evolution of the ethanol content as a function of time was observed with the other two V_f/V_s values (conditions (2) and (3) in Table 2). The concentration gradient reached by working with these

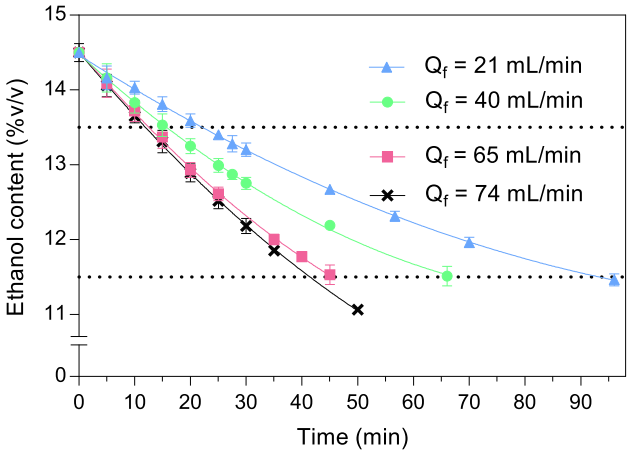

Fig. 4. Ethanol content as a function of time for a wine feed with 14.5 v/v% of ethanol and $V_f/V_s = 2$ and different feed flows; temperature = 21 °C. Represented data are the mean values with the corresponding standard deviations from a triplicated analytical measurement. The dotted lines represent the proposed dealcoholization grades (-3 v/v%) and (-1 v/v%) and the curves are only guides to the eye.

volume ratios allows the proposed degree of dealcoholization to be achieved with minimal differences in the operation time required (Fig. 3D). Thus, the optimal condition was set up at $V_f/V_s = 2$ to use a lower amount of stripping phase for an approximately loss of 3 alcoholic degrees. In addition, the stripping phase after the osmotic distillation is considered as a waste, or at least a stream needed of further treatment, representing an economic loss. Therefore, further improvement of this

Table 3
Theoretical mass transfer coefficients at different operation conditions.

Condition	$K_s \cdot 10^6$ (m s^{-1})	$K_f \cdot 10^6$ (m s^{-1})	$K_m \cdot 10^6$ (g m^{-2} s^{-1} Pa^{-1})	$K_G \cdot 10^6$ (g m^{-2} s^{-1} Pa^{-1})	Error (%)
1	9.57	2.91	210	31.8	1.8[a]
2	9.57	2.91	210	31.8	3.8[a]
3	9.57	2.91	210	31.8	4.5[a]
4	9.57	1.24	210	27.9	11.0[b]
5	9.57	2.02	210	30.4	8.3[c]
6	9.57	3.20	210	32.1	3.4[d]

[a] 45 min.
[b] 96 min.
[c] 66 min.
[d] 50 min.

process could be to obtain bioethanol from this waste with greater added value. In fact, in the latter case, it is possible to achieve a valorization of the stripping phase via distillation or pervaporation to obtain an alcohol-rich stream. In such case, the optimal condition ($V_f/V_s = 2$), giving rise to a higher permeate ethanol concentration than $V_f/V_s = 1$, would be more favorable from the energy point of view.

4.4. Influence of feed flow

Fig. 4 shows the variation of the ethanol content for the experiments carried out with $V_f/V_s = 2$. The stripping flow was set up at 39 mL min^{-1}, while the feed flow was varied between 21 and 74 mL min^{-1}. The effect of Q_s was not estudied in deph due to the lower influence on the ethanol transfer observed from water-ethanol experiments, in agreement with previous reported literature [40]. As Fig. 4 shows, an increment of the feed flow rate led to a faster decrease in the ethanol content of wine, what allowed to achieve the proposed goal (-3 v/v%) in 45 min at a Q_f of

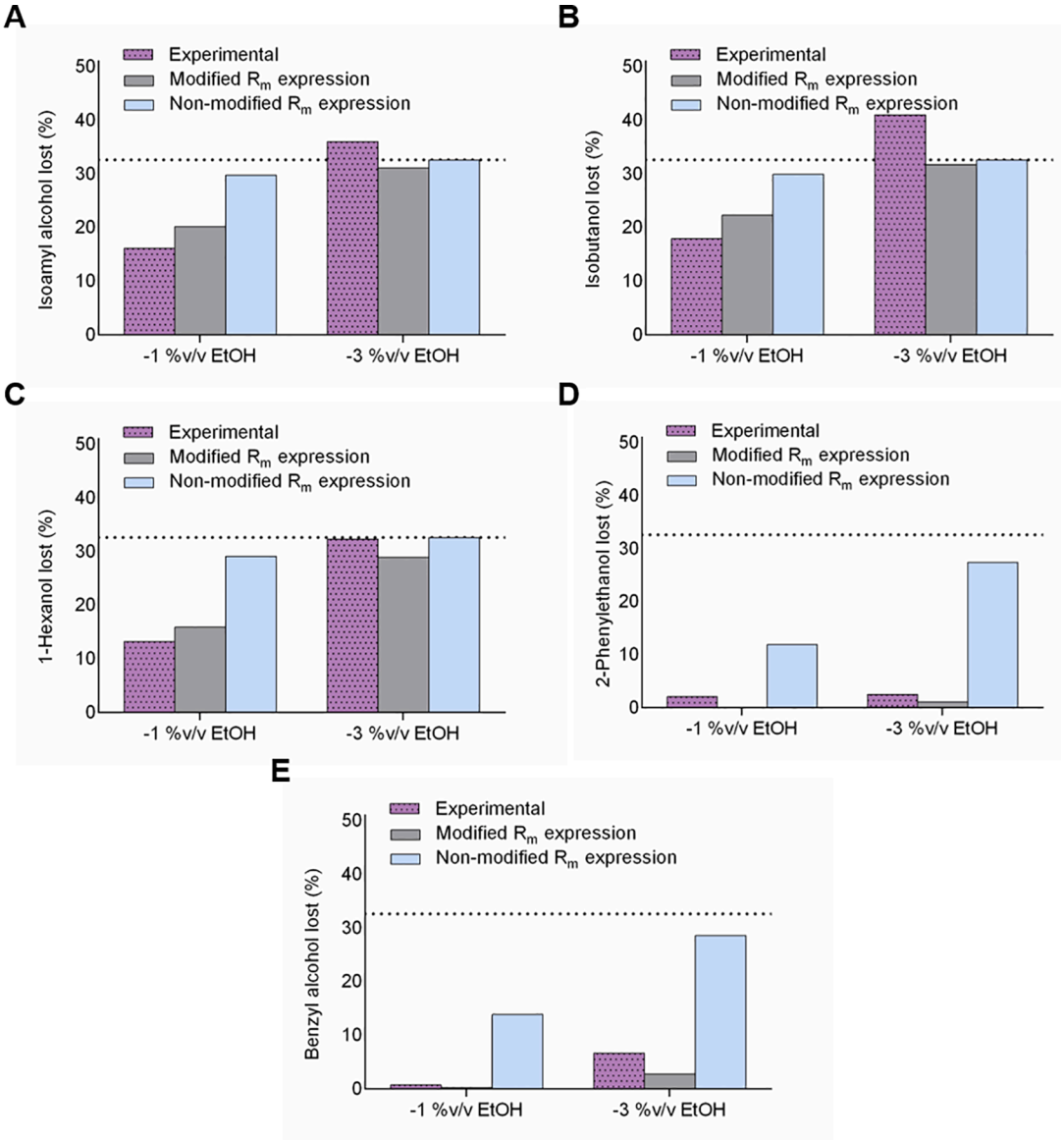

Fig. 5. Experimental and predicted losses of high alcohols from modified and non-modified R_m expression: (A) isoamyl alcohol, (B) isobutanol, (C) 1-hexanol, (D) 2-phenylethanol and (E) benzyl alcohol. The dotted line represents the steady state loss fixed by the ratio $V_f/V_s = 2$ (i.e. calculated from the mass balance when feed and stripping ethanol concentrations were equal); temperature = 21 °C.

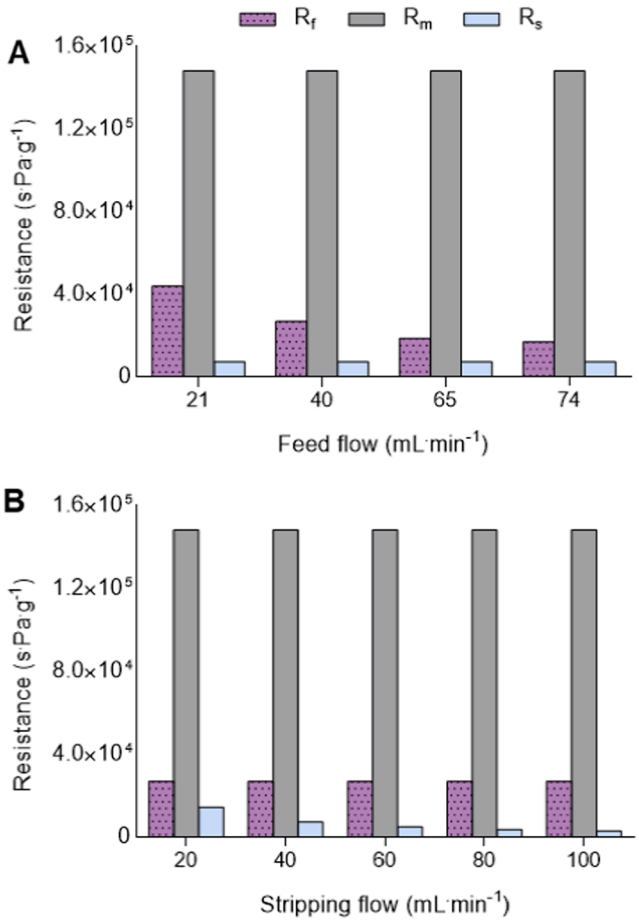

Fig. 6. Simulated contribution of each local resistance to the R_G for ethanol: (A) as a function of feed flow (Q_f) (conditions used in experiments 2, 4, 5 and 6, see Table 2); (B) results obtained varying the stripping flow (Q_s) in the 20–100 mL min^{-1} range.

74 mL min^{-1}. In addition, working with a feed flow above 74 mL min^{-1} did not have the expected increment of ethanol transport through the membrane. In consequence, it is not recommended to work with the current membrane area overpassing this flow.

4.5. Validation of theoretical model

Using the proposed mathematical model, the theoretical mass transfer coefficients (K_s^i, K_f^i, K_m^i and R_G^i) were calculated for ethanol (shown in Table 3). The error corresponding to the ethanol concentration was estimated as follows:

$$Error(\%) = \frac{C_{Exp,t}^{EtOH} - C_{Theo,t}^{EtOH}}{C_{Exp,t}^{EtOH}} \quad (15)$$

where $C_{Exp,t}^{EtOH}$ and $C_{Theo,t}^{EtOH}$ are the ethanol experimental and theoretical concentrations, respectively, at a given process time (see Table 3).

From the membrane resistance, K_m calculation gave a value of $2.1{\cdot}10^{-4}$ g m^{-2} s^{-1} Pa^{-1} which agrees with that obtained by Diban et al. [26,27], $1.6{\cdot}10^{-4}$ g m^{-2} s^{-1} Pa^{-1}. As explained above, Hansen solubility parameters were applied to modify R_m to account for the influence of each component-membrane interaction (Eq. (14)). To validate the model, our study was focused on the alcoholic components (thus, excluding esters and acids), optimizing φ coefficient to minimize the sum of the standard errors between the theoretical and experimental concentration values of ethanol and other five different high alcohol compounds. In particular, alcohols whose presence is majority in the wine, and differing on the length of the aliphatic chain and/or the functional group (i.e. isoamyl alcohol, isobutanol, 1-hexanol, 2-phenylethanol and benzyl alcohol) were studied. The goodness of the theoretical approach was determined based on the sum of errors, which was calculated as follows:

$$Error(\%) = \sum \left(\frac{C_{Exp}^i - C_{Theo}^i}{C_{Exp}^i} \right)^2 \quad (16)$$

An error of 4.3% was obtained using a φ value of 2.29, while the error was 30% from the non-modified R_m. Then, R_m modified values correlated better with the loss of all alcohols tested than non-modified R_m values, showing a lower difference between theoretical and experimental values in case of high alcohol losses (Fig. 5).

The losses of aliphatic alcohols (isoamyl alcohol, isobutanol and 1-hexanol) after a partial dealcoholization of 3 v/v% were close to the steady state ($J^{EtOH} = 0$), being adequately predicted by both models. However, at a lower degree of dealcoholization (1 v/v%), both models differ in their predictions. Thus, after reducing one degree of ethanol, the flux calculated using the non-modified R_m values was overestimated in all the aliphatic alcohols tested, while using the current model this overestimation was corrected. On the other hand, aromatic alcohols (2-phenylethanol and benzyl alcohol) showed an experimental behavior significantly different from that of the aliphatic alcohols tested due to their minor volatility and higher molar mass. This means that their fluxes depend mainly on R_m, what increases the difference between both theoretical predictions. Thus, for the two dealcoholization steps, the flux calculated using the non-modified R_m values was overestimated, while using the current (modified) model this overestimation was partially corrected. As can be seen in Fig. 5D and 5E, the model predictions for aromatic alcohols were not as good as for aliphatic alcohols, possibly related to the influence of aromatic ring on the –OH group.

Once the model to calculate the theoretical R_m values was optimized, the global mass transfer resistance was obtained to predict the ethanol transfer during dealcoholization process at different operating conditions. Fig. 6 depicts the theoretical estimation of each local resistance applied to calculate the global mass transfer resistance for ethanol. Fig. 6A and B show the results at different Q_f and Q_s conditions, respectively.

Fig. 6 demonstrates that high flows improve the hydrodynamic conditions minimizing the feed and stripping boundary layer resistances, locating the main resistance in the membrane. In addition, the influence of R_f becomes lower as the flow increases, giving rise to a global transfer resistance that is not dependent on the flow (Fig. 6A). Hence, from a certain flow, the resistance associated to the feed boundary layer reaches a minimum, maintaining the global transfer resistance independent from feed flow. Moreover, R_s shows the minor contribution comparing to the others (Fig. 6A and B) as mentioned above. These results are in agreement with our empirical observations (Fig. 4), and a similar tendency was found in previous experimental reports [27,40].

Graphical representations of the evolution of theoretical and experimental ethanol fluxes are shown in Figs. 7 and 8 to corroborate the suitability of the mathematical model. As can be seen, similar theoretical trends and values to the experimental ones can be inferred from these figures, in line with the reduced ethanol concentration error reported in Table 3. Besides, the experimental fluxes easily achieved from the weight gained by the stripping phase are similar to those obtained from the chromatographic analyses, meaning the mass transfer corresponds almost exclusively to ethanol. The largest deviation between the simulated curves and the experimental values as a function of V_f/V_s ratio can be appreciated in condition (1) (Fig. 7A, Table 2) where the ethanol permeation flux almost reached steady state as Fig. 3A suggested.

The influence of the Q_f/Q_s ratio on the variation of the ethanol content was also adequately predicted by the mathematical model as Fig. 8 depicts, although it is noticeable that at low feed flow rates

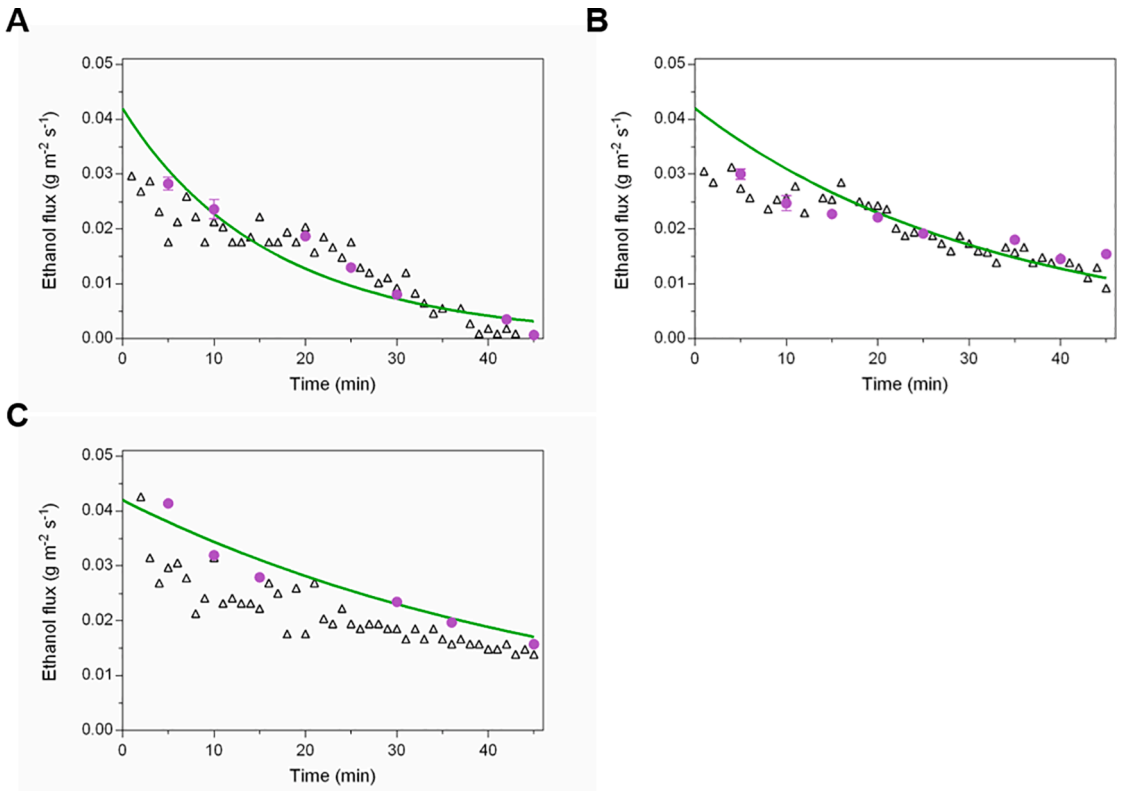

Fig. 7. Mass fluxes as a function of time for 375 mL of wine with 14.5 v/v% of ethanol at different volume ratios between feed and stripping phases (V_f/V_s): (A) 5, (B) 2, (C) 1. T = 21 °C. Q_f = 65 mL min^{-1}, Q_s = 39 mL min^{-1}. Green continuous lines represent the ethanol flux predicated by the model. Circles coincide with experimental ethanol mean values with the corresponding standard deviations (very small to be shown) from a triplicated chromatographic analytical measurement. Triangles represent the experimental total flux; determined by means of the stripping weight.

(Fig. 8A), the predicted results slightly deviate from the experimental values. This may be due to the influence of the concentration polarization on the ethanol flux, which has not been taken into account in the theoretical model.

Finally, Fig. 9 compiles a set of 11 experiments carried out under the same experimental conditions and using the same polypropylene hollow fiber membrane module (in fact, the module was applied in more than 20 experiments) to dealcoholize both water-ethanol solutions and the tempranillo wine. No important changes in ethanol permeation fluxes are appreciated with an average value of permeation flux of 0.025 ± 0.005 g m^{-2} s^{-1}. This suggests that the permeation flux was unaffected by the type feed (either hydro alcoholic solutions or red wines) but also by a possible fouling generated during every experiment, having in mind that the hollow fiber membrane modules were submitted to an exhaustive cleaning protocol (water-NaOH solution-water treatments followed by drying evacuation and N_2 flushing) after every use, as described in the experimental section. In summary, this allows to discard membrane fouling along the cumulative operation of the hollow fiber membrane module.

5. Conclusions

A partial dealcoholization of wine was successfully carried out by osmotic distillation (OD) using a polypropylene hollow fiber membrane module with a membrane area of 0.18 m^2. The feasibility of the approach was first established using water-ethanol solutions, whose results showed a good correlation with those obtained with tempranillo red wine. This variety was used to study the influence of different experimental conditions on the ethanol mass transfer observed during dealcoholization. The best results were obtained at feed/stripping volume ratio = 2 and feed flow = 74 mL min^{-1}.

Furthermore, a mathematical model was proposed to predict the OD performance, obtaining an error as small as 4.3% in the prediction of alcohol losses. In this model, the membrane resistance expression, based on the so-called dusty gas model, was modified including a component-membrane specific interaction that allowed to describe the components behavior when permeating through the membrane as a function of their volatilities (Henry's constants) and their interactions with the membrane material in terms of Hansen solubility parameters (*HSP*).

The behavior of ethanol and other five high alcohols whose presence is majority in the wine was studied to develop the proposed membrane resistance expression. In addition, it was shown that the calculated membrane resistance (modified by the inclusion of Hansen solubility parameters, *HSP*) allowed an adequate prediction for alcohols with low Henry's constant (i.e. the aliphatic alcohols studied here), while it was slightly overestimated for alcohols with high Henry's constant such as 2-phenylethanol and benzyl alcohol. It is worth noticing that the *HSP* based modification gave rise to relatively small errors when experimental and theoretical ethanol concentrations were compared in a relatively wide range of operating conditions, and also when experimental and theoretical high alcohols concentrations were compared at the best working conditions in terms of feed flow, feed/stripping volume ratio and dealcoholization degree.

Finally, the stable operation of the polypropylene hollow fiber membrane module was demonstrated through its use in more than 20 dealcoholization experiments with both water-ethanol solutions and red wine.

Credit authorship contribution statement

Javier Esteras-Saz: Conceptualization, Data curation, Formal analysis, Investigation, Methodology, Project administration, Validation, Writing - original draft, Review & editing. **Óscar de la Iglesia:** Conceptualization, Formal analysis, Methodology, Validation, Writing -

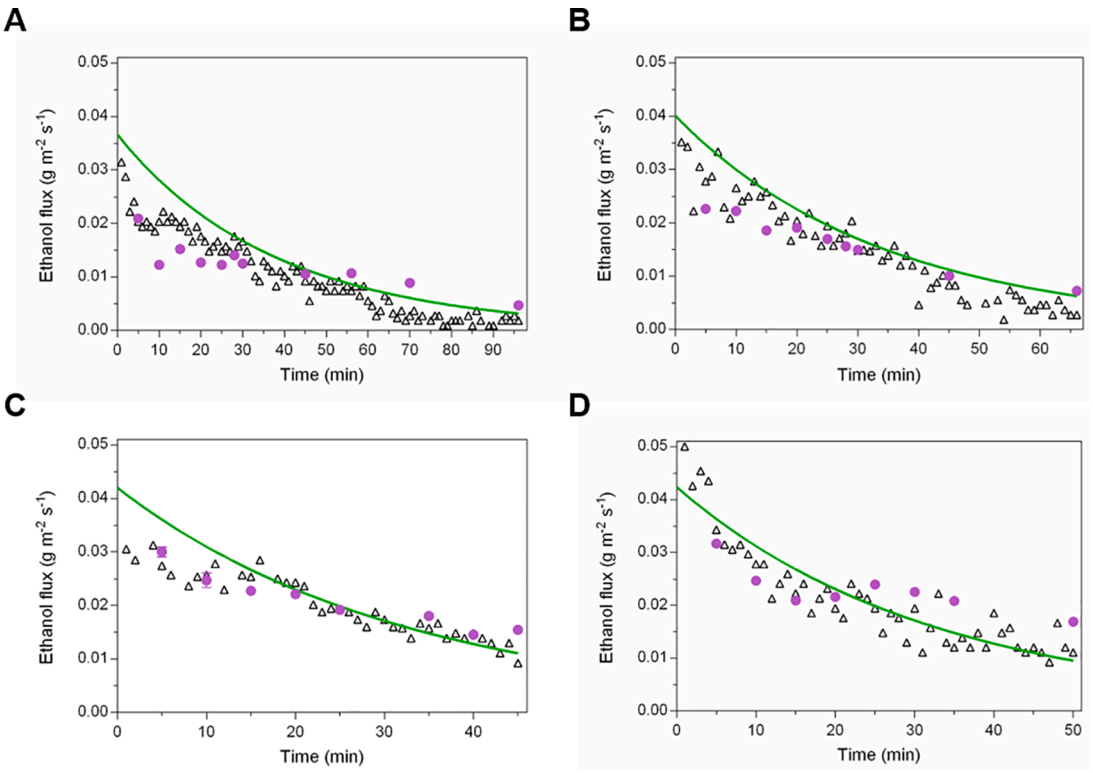

Fig. 8. Ethanol flux as a function of time for a wine with 14.5 v/v of ethanol at stripping flow of 39 mL min^{-1} and different feed flows (Q_f): (A) 21 mL min^{-1}, (B) 39 mL min^{-1}, (C) 65 mL min^{-1}, (D) 74 mL min^{-1}. ($V_f = 375$ mL, $V_s = 187.5$ mL, T = 21 °C). Green continuous lines represent the ethanol flux predicated by the model. Circles coincide with experimental ethanol mean values with the corresponding standard deviations (very small to be shown) from a triplicated chromatographic analytical measurement. Triangles represent the experimental total flux; determined by means of the stripping weight.

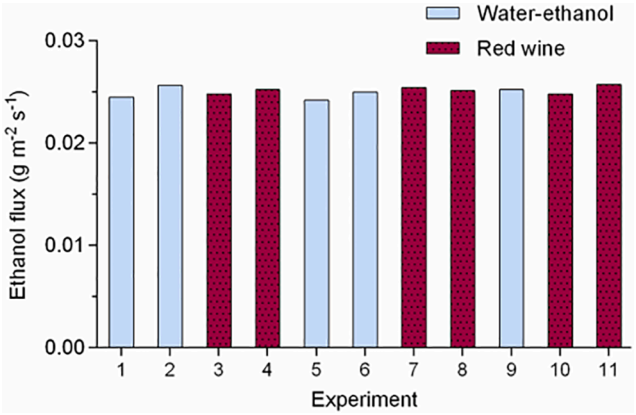

Fig. 9. Ethanol flux at 25 min obtained for 11 dealcoholization experiments carried out using the same hollow fiber membrane module under the same operation conditions of $V_f = 250$ mL; $V_s = 125$ mL; $Q_f = 74$ mL min^{-1}; $Q_s = 39$ mL min^{-1}.

original draft, Review & editing, Supervision. **Cristina Peña:** Conceptualization, Data curation, Formal analysis, Investigation, Methodology, Validation, Writing - original draft, Review & editing. **Ana Escudero:** Conceptualization, Funding acquisition, Project administration, Validation, Writing - original draft, Validation, Review & editing, Supervision. **Carlos Téllez:** Conceptualization, Validation, Writing - original draft, Validation, Review & editing, Supervision. **Joaquín Coronas:** Conceptualization, Funding acquisition, Project administration, Validation, Writing - original draft, Validation, Review & editing, Supervision.

Declaration of Competing Interest

The authors declare that they have no known competing financial interests or personal relationships that could have appeared to influence the work reported in this paper.

Acknowledgements

Financial support from FEDER/Ministerio de Ciencia, Innovación y Universidades – Agencia Estatal de Investigación (Spain)/RTC-2017-6360-2 is gratefully acknowledged.

Appendix A. Supplementary material

Supplementary data to this article can be found online at https://doi.org/10.1016/j.seppur.2021.118793.

References

[1] T.R. Carter, M.L. Parry, J.H. Porter, Climatic change and future agroclimatic potential in Europe, Int. J. Climatol. 11 (1991) 251–269.
[2] M.P. McCarthy, M.J. Best, R.A. Betts, Climate change in cities due to global warming and urban effects, Geophys. Res. Lett. 37 (2010) L09705.
[3] B.B. Hansen, V. Grøtan, I. Herfindal, A.M. Lee, The Moran effect revisited: spatial population synchrony under global warming, Ecography (Cop.) 43 (2020) 1591–1602.
[4] F. Zamora, Elaboración y crianza del vino tinto: Aspectos científicos y prácticos, 2003rd ed., Madrid, 2003.
[5] N.H. Mermelstein, Removing alcohol from wine, Food Technol. 54 (2000) 89.
[6] G.V. Jones, M.A. White, O.R. Cooper, K. Storchmann, Climate change and global wine quality, Clim. Change. 73 (2005) 319–343.
[7] F. Zamora, Las manoproteínas; origen e interés enológico, Enólogos. 39 (2005) 28–31.
[8] J. Drappier, C. Thibon, A. Rabot, L. Geny-Denis, Relationship between wine composition and temperature: impact on Bordeaux wine typicity in the context of global warming—Review, Crit. Rev. Food Sci. Nutr. 59 (2019) 14–30.

[9] International Organisation of Vine and wine (OIV), OIV Rules and implications concerning reduction of alcohol levels. Alcohol level reduction in Wine. Oenoviti International Network. 1st International Symposium. ISVV, Villenave d'Ornon, France, (2013).
[10] P. Godden, E. Wilkes, D. Johnson, Trends in the composition of Australian wine 1984–2014, Aust. J. Grape Wine Res. 21 (2015) 741–753.
[11] J. Wang, X. Zhang, L. Su, H. Li, L. Zhang, J. Wei, Global warming effects on climate zones for wine grape in Ningxia region, China, Theor. Appl. Climatol. 140 (2020) 1527–1536.
[12] M.C. Goldner, M.C. Zamora, P. Di Leo Lira, H. Gianninoto, A. Bandoni, Effect of ethanol level in the perception of aroma attributes and the detection of volatile compounds in red wine, J. Sens. Stud. 24 (2009) 243–257.
[13] A.L. Robinson, S.E. Ebeler, H. Heymann, P.K. Boss, P.S. Solomon, R.D. Trengove, Interactions between wine volatile compounds and grape and wine matrix components influence aroma compound headspace partitioning, J. Agric. Food Chem. 57 (2009) 10313–10322.
[14] B. Pineau, J.C. Barbe, C. Van Leeuwen, D. Dubourdieu, Examples of perceptive interactions involved in specific "Red-" and "Black-berry" aromas in red wines, J. Agric. Food Chem. 57 (2009) 3702–3708.
[15] M. Rosell, U. de Faire, M.L. Hellénius, Low prevalence of the metabolic syndrome in wine drinkers - is it the alcohol beverage or the lifestyle? Eur. J. Clin. Nutr. 57 (2003) 227–234.
[16] O.J. Schelezki, A. Deloire, D.W. Jeffery, Substitution or dilution? Assessing pre-fermentative water implementation to produce lower alcohol Shiraz wines, Molecules 25 (2020) 2245.
[17] S. Dequin, J.-L. Escudier, M. Bely, J. Noble, W. Albertin, I. Masneuf-Pomarède, P. Marullo, J.-M. Salmon, J.M. Sablayrolles, How to adapt winemaking practices to modified grape composition under climate change conditions, OENO One 51 (2017) 205–214.
[18] M.A. Olego, F. Visconti, M.J. Quiroga, J.M. de Paz, E. Garzón-Jimeno, Assessing the effects of soil liming with dolomitic limestone and sugar foam on soil acidity, leaf nutrient contents, grape yield and must quality in a mediterranean vineyard, Spanish J. Agric. Res. 14 (2016), e1102.
[19] M. Catarino, A. Mendes, L.M. Madeira, A. Ferreira, Alcohol removal from beer by reverse osmosis, in: Sep. Sci. Technol., 2007: pp. 3011–3027.
[20] L.M. Schmidtke, J.W. Blackman, S.O. Agboola, Production technologies for reduced alcoholic wines, J. Food Sci. 77 (2012) R25–R41.
[21] L. Liguori, P. Russo, D. Albanese, M. Di Matteo, Evolution of quality parameters during red wine dealcoholization by osmotic distillation, Food Chem. 140 (2013) 68–75.
[22] O. Corona, L. Liguori, D. Albanese, M. Di Matteo, L. Cinquanta, P. Russo, Quality and volatile compounds in red wine at different degrees of dealcoholization by membrane process, Eur. Food Res. Technol. 245 (2019) 2601–2611.
[23] M.T. Lisanti, A. Gambuti, A. Genovese, P. Piombino, L. Moio, Partial dealcoholization of red wines by membrane contactor technique: effect on sensory characteristics and volatile composition, Food Bioprocess Technol. 6 (2013) 2289–2305.
[24] R. Prasad, K.K. Sirkar, Dispersion-free solvent extraction with microporous hollow-fiber modules, AIChE J. 34 (1988) 177–188.
[25] K.H. Keller, T.R. Stein, A two-dimensional analysis of porous membrane transport, Math. Biosci. 1 (1967) 421–437.
[26] N. Diban, V. Athes, M. Bes, I. Souchon, Ethanol and aroma compounds transfer study for partial dealcoholization of wine using membrane contactor, J. Membr. Sci. 311 (2008) 136–146.
[27] N. Diban, A. Arruti, A. Barceló, M. Puxeu, A. Urtiaga, I. Ortiz, Membrane dealcoholization of different wine varieties reducing aroma losses. Modeling and experimental validation, Innov. Food Sci. Emerg. Technol. 20 (2013) 259–268.
[28] L. Liguori, P. Russo, D. Albanese, M. Di Matteo, Effect of process parameters on partial dealcoholization of wine by osmotic distillation, Food Bioprocess Technol. 6 (2013) 2514–2524.
[29] C. Ortega, R. López, J. Cacho, V. Ferreira, Fast analysis of important wine volatile compounds - development and validation of a new method based on gas chromatographic-flame ionisation detection analysis of dichloromethane microextracts, J. Chromatogr. A. 923 (2001) 205–214.
[30] L. Liguori, D. Albanese, A. Crescitelli, M. Di Matteo, P. Russo, Impact of dealcoholization on quality properties in white wine at various alcohol content levels, J. Food Sci. Technol. 56 (2019) 3707–3720.
[31] A. Gabelman, S.T. Hwang, Hollow fiber membrane contactors, J. Membr. Sci. 159 (1999) 61–106.
[32] S. Bocquet, F. Gascons Viladomat, C. Muvdi Nova, J. Sanchez, V. Athes, I. Souchon, Membrane-based solvent extraction of aroma compounds: choice of configurations of hollow fiber modules based on experiments and simulation, J. Membr. Sci. 281 (2006) 358–368.
[33] S. Shen, S.E. Kentish, G.W. Stevens, Shell-side mass-transfer performance in hollow-fiber membrane contactors, Solvent Extr. Ion Exch. 28 (2010) 817–844.
[34] V.D. Alves, I.M. Coelhoso, Effect of membrane characteristics on mass and heat transfer in the osmotic evaporation process, J. Membr. Sci. 228 (2004) 159–167.
[35] R.H. Perry, Perry's Chemical Engineers' Handbook, seventh ed., McGraw-Hill, New York, 2001.
[36] A. Baudot, J. Floury, H.E. Smorenburg, Liquid-liquid extraction of aroma compounds with hollow fiber contactor, AIChE J. 47 (2001) 1780–1793.
[37] C.M. Hansen, Polymer additives and solubility parameters, Prog. Org. Coatings 51 (2004) 109–112.
[38] C.M. Hansen, Aspects of solubility, surfaces and diffusion in polymers, Prog. Org. Coatings 51 (2004) 55–66.
[39] M.H. Charles, Hansen Solubilities Parameters, CRC Press, Boca Ratón, 2013.
[40] S. Varavuth, R. Jiraratananon, S. Atchariyawut, Experimental study on dealcoholization of wine by osmotic distillation process, Sep. Purif. Technol. 66 (2009) 313–321.